




ARTICLE



L1CAM and laminin vascular network: Association with the high-risk replacement histopathologic growth pattern in uveal melanoma liver metastases

Raymond Barnhill ^{1,2✉}, Steven van Laere³, Peter Vermeulen³, Sergio Roman-Roman¹, Sophie Gardrat⁴, Samar Alsafadi¹, Malcy Tarin¹, Gabriel Champenois⁴, André Nicolas⁴, Alexandre Matet^{2,5}, Nathalie Cassoux^{2,5}, Vincent Servois⁶, Manuel Rodrigues^{7,8}, Richard Scolyer ^{9,10,11,12}, Alexander Lazar ¹³, Emanuela Romano⁷, Sophie Piperno-Neumann⁷, Pascale Mariani¹⁴ and Claire Lugassy¹

© The Author(s), under exclusive licence to United States and Canadian Academy of Pathology 2022

The replacement histopathologic growth pattern (rHGP) in melanoma liver metastases connotes an aggressive phenotype (vascular co-option; angiotropic extravascular migratory spread) and adverse prognosis. Herein, replacement and desmoplastic HGP (dHGP) were studied in uveal melanoma liver metastases (MUM). In particular, L1CAM and a “laminin vascular network” were detected at the advancing front of 14/20 cases ($p = 0.014$) and 16/20 cases ($p = 6.4e-05$) rHGPs, respectively, but both were absent in the dHGP (8/8 cases) ($p = 0.014$, and $p = 6.3e-05$, respectively). L1CAM highlighted progressive extension of angiotropic melanoma cells along sinusoidal vessels in a pericytic location (pericytic mimicry) into the hepatic parenchyma. An inverse relationship between L1CAM expression and melanin index ($p = 0.012$) suggested differentiation toward an amelanotic embryonic migratory phenotype in rHGP. Laminin labeled the basement membrane zone interposed between sinusoidal vascular channels and angiotropic melanoma cells at the advancing front. Other new findings: any percentage of rHGP and pure rHGP had a significant adverse effect on metastasis-specific overall survival ($p = 0.038$; $p = 0.0064$), as well as predominant rHGP ($p = 0.0058$). Pure rHGP also was associated with diminished metastasis-free survival relative to dHGP ($p = 0.040$), possibly having important implications for mechanisms of tumor spread. In conclusion, we report for the first time that L1CAM and a laminin vascular network are directly involved in this high-risk replacement phenotype. Further, this study provides more detailed information about the adverse prognostic effect of the rHGP in MUM.

Laboratory Investigation (2022) 102:1214–1224; <https://doi.org/10.1038/s41374-022-00803-w>

INTRODUCTION

Up to 50% of primary uveal melanomas (PUM) metastasize to the liver. Despite objective and reproducible risk stratification of patients with PUM^{1–3}, overall survival is dismal. In addition, high-risk genetic alterations (loss of chromosome 3 and gain in chromosome 8q) observed in PUM appear to have no prognostic value once liver metastases have developed (see below, 4). Furthermore, molecular characterization of UM liver metastases (MUM) has not yet targeted critical regions of these metastases in tissue samples. As a result, there is an urgent need for spatial characterization of specific microscopic regions of high-risk MUM and the development of effective therapies for MUM.

We have recently studied for the first time histopathological growth patterns (HGPs) in 41 patients with UM liver metastases⁴, employing international consensus guidelines established for

metastases originating from all solid tumors such as colorectal carcinoma⁵. The principal patterns are “replacement” and “desmoplastic”. The replacement HGP (rHGP) is defined by tumor cells that infiltrate and replace hepatocytes at the peritumoral-stromal interface, i.e., the advancing front of the metastasis, in a “pericytic” location along the co-opted abluminal surfaces of sinusoidal vessels or venules of the portal tracts. This pattern corresponds to angiotropism and pericytic mimicry (PM) of tumor cells and their migration along vessels at the advancing front of the tumor^{6,7} (see below). In contrast, the desmoplastic HGP (dHGP) is defined by a distinct separation of the metastasis from the liver parenchyma by a peripheral annulus (rim) of desmoplastic fibrous tissue. Importantly, liver metastases from colorectal carcinoma with the replacement HGP are associated with an adverse prognosis and resistance to treatment, while the dHGP connotes a favorable prognosis^{8,9}.

¹Department of Translational Research, Institut Curie, Paris, France. ²Université de Paris UFR de Médecine, Paris, France. ³Faculty of Medicine and Health Sciences, University of Antwerp—MIPRO Center for Oncological Research (CORE)—TCRU, GZA Sint-Augustinus, Antwerp, Belgium. ⁴Department of Pathology, Institut Curie, Paris, France. ⁵Department of Ophthalmology, Institut Curie, Paris, France. ⁶Department of Radiology, Institut Curie, Paris, France. ⁷Department of Medical Oncology, Institut Curie, Paris, France. ⁸Inserm U830, DNA Repair and Uveal Melanoma (D.R.U.M.), Equipe Labellisée Par la Ligue Nationale Contre le Cancer, Institut Curie, Paris, France. ⁹Melanoma Institute of Australia, Sydney, NSW, Australia. ¹⁰Faculty of Medicine and Health, The University of Sydney, Sydney, NSW, Australia. ¹¹Tissue Pathology and Diagnostic Oncology, Royal Prince Alfred Hospital and NSW Health Pathology, Sydney, NSW, Australia. ¹²Charles Perkins Centre, The University of Sydney, Sydney, NSW, Australia. ¹³Department of Pathology and Genomic Medicine, The University of Texas M.D. Anderson Cancer Center, Houston, TX, USA. ¹⁴Department of Surgery, Institut Curie, Paris, France. ✉email: raymond.barnhill@curie.fr

Received: 10 March 2022 Revised: 25 April 2022 Accepted: 2 May 2022

Published online: 7 June 2022

The pushing HGP, which is much less common to rare, is characterized by compression of the liver parenchyma by expansile growth of the metastasis⁵.

In our previous study of MUM, 73% of the cases exhibited a predominate (> 50%) replacement HGP and an adverse prognosis^{4,7}. In contrast, 27% of the MUM were predominately desmoplastic and had a more favorable prognosis. On multivariate analysis, HGP status (hazard ratio; HR = 6.51, $p = 0.008$) remained significant, whereas the high-risk genetic variable monosomy 3/8q gain had no predictive value. These findings are directly comparable to those for other solid tumors and provide for the first time an important tissue biomarker for prognosis after the development of liver metastases in UM. We have also recently confirmed very similar results in liver metastases from cutaneous melanoma⁸.

The advancing front of the replacement pattern, which is associated with angiotropic tumor cell migration in the space of Disse, represents a critical microenvironment for neoplastic progression. This perivascular space is a preferential niche for cancer stem cells (CSC), leading to resistance to therapy, protection or escape from the immune response, and the progression and dissemination of cancer⁷⁻¹⁰.

For more than two decades, L1CAM (L1 cell adhesion molecule), a transmembrane glycoprotein, has been shown to play an important role in cell migration, adhesion, differentiation, in cancer development and metastases, and is associated with a poor prognosis¹¹. L1CAM has been shown to bind to laminin¹² and to be involved in haptotaxis, i.e., cell migration directed by substrate-bound chemical cues¹³. Notably, grip and slip between L1CAM and the adhesive substrates that direct growth cone migration is mediated by laminin¹⁴. L1CAM has been implicated in the outgrowth of metastases from several cancers by enabling adhesion of cancer cells to laminin-rich basement membrane with tumor cells mimicking pericytes and spreading along vascular channels, i.e., PM^{15,16}.

Remodeling of laminins triggers new interactions with cell-surface receptors and cytoplasmic signaling pathways responsible for a variety of biological processes among which are cell migration, outgrowth, and metastasis^{7,9,17-19}. In particular, laminin is essential during vasculature-guided neuronal migration, a physiological post-natal process analogous to PM²⁰. Migration of glioblastoma cells along vessels into the brain, which seems closely related to physiological neuronal migration²¹, appears dependent upon a laminin isoform shift²². Taken together, these data indicate that critical signaling pathways linked to L1CAM and laminin could be localized to the advancing front of MUM with the replacement HGP.

Our objectives in the current study were (i) to investigate the localization of L1CAM and laminin at the invasive front of the replacement HGP versus that of the more favorable desmoplastic type; and (ii) to provide more information about the adverse prognostic of the rHGP in MUM.

MATERIALS/SUBJECTS AND METHODS

This study was approved by the institutional ethics committee of Institut Curie. Written informed consent for the use of tissue specimens and data for research was signed by each patient. The study complied with the principles of the Declaration of Helsinki.

Patient information

Seventy-two hepatic metastases resected from 72 patients with uveal melanoma (UM) were enrolled in the study based on adequate material available for histopathological examination (see below). Sixty-three cases with MUM from the period 2007 to 2017 from Institut Curie (IC), 8 cases from the University of Texas MD Anderson Cancer Center from the period of 2000 to 2018 and 1

Table 1. Patient and primary uveal melanoma characteristics.

Patient characteristics	n = 72 (%)
Gender (female),	34 (47%)
Age at diagnosis, years	
Mean (sd)	53.9 (11.4)
Median (range)	54 (30–78)
Primary tumor characteristics	n = 63
Largest tumor diameter (LTD), mm (MD = 12)	
Mean (sd)	16.0 (3.3)
Median (range)	16 (6–22)
Melanoma cell type (n = 32) (MD = 40)	
- epithelioid	8 (25%)
- spindle	8 (25%)
- mixed	16 (50%)
Local extension (n = 62) (MD = 10)	
- no	51 (82%)
- ciliary body	10 (16%)
- optic nerve	1 (2%)
- extrascleral	0 (0%)
Array CGH* (n = 62) (MD = 10)	
D3/8 N	3 (5%)
M3/8 N	5 (8%)
D3/8 G	18 (29%)
M3/8 G	36 (58%)
BAP1 mutation (n = 56) (MD = 16),	39 (69.6%)
Local treatment (n = 63) (9)	
- enucleation	32 (51%)
- proton beam	28 (44%)
- iodine disc brachytherapy	3 (5%)
- fine-needle aspiration	0 (0%)

*Cassoux Risk Group: Four genomic groups defined by the status of chromosome 3 and 8q: (1) Low risk: normal status of chromosomes 3 (disomy 3) and 8q (8 N): D3/8 N, (2) Intermediate risk: monosomy 3 and normal status of 8q: M3/8 N, (3) Intermediate risk: disomy 3 and gain of 8q (8 G): D3/8 G, and (4) High risk: M3/8 G²⁷.

case from the Melanoma Institute of Australia from 2018 were retrieved from the anatomic pathology archives of the three institutions. Only completely resected surgical specimens were entered into the study. Needle biopsies were excluded. Comprehensive clinical, histopathologic, and genetic information (see Supplementary information) with reference to both primary and metastatic tumor specimens were collected.

The following patient and PUM characteristics are displayed in Table 1: age (years); gender; largest tumor diameter (LTD) of the primary uveal melanoma (in mm); melanoma cell type (Histotype; modified Callender classification²³: epithelioid, spindle, or mixed²⁴; local extension of the primary tumor (ciliary body, optic nerve, or extrascleral extension); genetic analysis (see below); BAP1 mutation status (see below); local therapy of the PUM (proton beam therapy, radioactive (iodine) disc brachytherapy, enucleation); R (resection) status of metastasis: R0 - resection complete, R1 - microscopically incomplete, R2 - macroscopically incomplete; initial (first) therapy of liver metastases (surgery alone for limited metastatic disease, systemic therapy alone, best support care (no specific therapy)); and survival (see below). Other variables describing the metastatic disease status such as tumor burden (number or size of metastases per se, serum LDH) or performance status were not studied.

Histopathologic analysis

Formalin-fixed, paraffin-embedded (FFPE) 5- μ m sections were prepared for each liver metastasis and stained with hematoxylin-eosin-saffron (HES) (IC only) or hematoxylin-eosin (H&E) for microscopic examination. Whole glass slides were digitized with a Phillips pathology slide scanner (Phillips Healthcare, Amsterdam, the Netherlands). Criteria for inclusion of MUMs in the study were as follows: the presence of a 360-degree circumference surrounded by viable intact liver parenchyma, or the highest percentage of the peripheral circumference of the MUM surrounded by liver parenchyma, and absence of significant necrosis, scarring, or disruption of either the metastasis or the liver. Histopathologic characteristics recorded based on the examination of representative HES- or H&E-stained sections or digital images for each case included: the histopathologic growth pattern (HGP) according to consensus guidelines⁵, angiotropism of melanoma cells, and the melanin content (see below) of the metastasis. The specific type of HGP was determined by histopathological examination of the tumor-peritumoral interface (or advancing front) with the surrounding liver parenchyma (see Introduction and ref.⁵). This interface or advancing front is a circumferential annulus of variable thickness ranging from ~1 to 4 mm and including a peripheral rim of tumor cells, a desmoplastic rim (if present), and surrounding hepatocytes. HGP assessment consisted of recording the percentage of the circumference involved (at least 5%) by replacement, desmoplastic, or pushing HGP. When more than one growth pattern was present in a metastasis, the relative fraction of each growth pattern as a percentage of the total length of the interface was estimated. The HGPs were analyzed in three groups as follows: (1) HGP1: predominant growth pattern (>50% of the circumference was replacement or desmoplastic), (2) HGP2: 100% (pure) desmoplastic vs. any replacement, and (3) HGP3: 100% (pure) replacement vs. any desmoplastic. Angiotropism was defined as previously described⁷. The images were reviewed independently by two experienced senior pathologists (RB and PV) without specific knowledge of the case or clinical outcome.

Melanin index (melanin content) of each metastasis was recorded according to the method developed by ref.²⁵ percentage of tumor containing melanin (range 0–100%), intensity of cytoplasmic melanin (0 - absent, 1- faint, 2- moderate, 3 - high, 4 - very high)²⁶, and melanin index (percentage melanin \times intensity = index (0 to 400)).

Genetic analysis²⁷ (see Supplementary information)

Immunohistochemical analysis

Analysis of BAP1 mutation: FFPE sections from 56 MUM were examined by immunohistochemistry for BAP1 expression (Dako, clone M0823, dilution 1/100). Tissue for 7 specimens was not available for study. A Vector Red chromogen was utilized for BAP1. Peroxidase activity was developed using 3-amino-9-ethylcarbazole and H₂O₂, and the slides were counterstained with hematoxylin.

Analysis of L1CAM and Laminin: Routinely fixed, paraffin-embedded, 3 μ m-thick tissue sections from 28 uveal melanoma liver metastases, including 20 MUM with >50 to 100% rHGP and 8 with >50 to 100% dHGP. Twenty-four MUM with sufficient tumor were available for study from the 63-patient cohort and four MUM were new recent cases from IC: 3 cases with 85 to 100% rHGP and 1 case with 100% dHGP. The tissue sections were de-paraffinized, rehydrated and pretreated by Proteinase K (5 min, 37 °C). L1CAM (Biologend, clone 14.10, 826701 (dilution 1/200)) and generic laminin (Sigma, L9393-100UL) detection by alkaline phosphatase technique and FAST-RED chromogenic substrate revelation on the BOND RX using the Bond Polymer Refine Red Detection Kit (Leica) according to the protocols recommended by the manufacturer: After blocking endogenous peroxidase activity and inhibiting non-specific staining, the slides were incubated with each diluted

antibody for 60 min at room temperature. Tissue sections were then washed with PBS and incubated with Poly-AP IgG reagent to localize rabbit antibodies. Immunoreactive signals were detected using 3-amino-4-methoxybenzidine (FAST RED) chromogen. Finally, the sections were lightly counterstained with Mayer's hematoxylin for 3 min.

L1CAM and laminin expression were assessed semi-quantitatively at the tumor-liver peritumoral interface. The percentage of tumor cells showing membranous expression of L1CAM were recorded at the advancing front of the metastasis. In a similar fashion, the percentage of the advancing front demonstrating a "laminin vascular network pattern" of expression involving the sinusoidal vascular channels interfacing with tumor cells was recorded. The laminin vascular network is defined by conspicuous immunostaining of laminin interposed between endothelial cells of sinusoidal vascular channels and angiotropic tumor cells at the advancing front of the MUM. The resulting image corresponds to a vascular network. The following method was used for scoring both L1CAM and laminin: 0 = absence of expression; 1+ = rare, or <1% expression of tumor cells or the "laminin vascular network" at the advancing front; 2+ = < 25% expression; 3+ = 25 to 50% expression; 4+ = > 50% expression.

Statistical analysis

Data were analyzed using R statistical software (<https://cran.r-project.org>). The relationships between HGPs and categorical variables were evaluated by linear regression, the Fisher Exact Test (*p* values and Odds ratios) and HGPs and continuous variables by the Mann–Whitney *U*-test (*p* values and fold changes as the ratio of replacement over desmoplastic HGP). The relationships between the percentage of L1CAM and laminin expression at the advancing front of both replacement and desmoplastic HGPs and melanin index were analyzed by the Kruskal–Wallis test. The survival analyses included metastasis-specific overall survival (MSOS), overall survival (OS), and metastasis-free survival (MFS; interval or time to metastasis) in months. MSOS was defined as the interval between the date at diagnosis of liver metastases (MUMs) and the date of death or at last follow-up. OS was defined as the interval between the date at diagnosis of the primary tumor and the date of death or at last follow-up. MFS was defined as the interval between the date at diagnosis of the primary tumor and the date of diagnosis of the MUM. MSOS, OS, and MFS were analyzed with special reference to histopathologic growth patterns groups HGP1, HGP2, and HGP2 and monosomy 3 and disomy 3 (see Supplementary data). In addition, the effects of all prognostic variables, especially various combinations of arrayCGH profiling groups 1–4 (defined above in Genetic analysis) and the new arrayCGH groups (aCGHgr1 – 5, defined in Supplementary Table 1) on MSOS and OS were examined.

Patients were censored when alive at last follow-up or when lost to follow-up. Differences in survival were calculated using the log-rank test. Univariate and multivariate hazard ratios were calculated using the Cox proportional hazards model. All statistical tests were considered significant with *p*-value < 0.05.

RESULTS

Clinical and other findings

The patient clinical information and primary tumor characteristics for 72 patients are summarized in Table 1.

Thirty-four women and 38 men constituted the study population with age mean = 53.9 years and median = 54 years (range: 30–78). Primary melanoma tumor diameter was mean = 16.0 mm, median = 16 mm (range: 6 to 22 mm). Twenty-four (75%) of the 32 cases with melanoma cell type available had an epithelioid or mixed phenotype versus only 8 cases (25%) with spindle cell type. Invasion of the ciliary body and optic nerve were observed in 10

Table 2. Distribution of histopathological growth patterns in uveal melanoma liver metastases.

Histopathological growth pattern	n = 72 (%)
Pure vs mixed pattern	
Replacement (pure, 100%)	39 (54.2%)
Desmoplastic (pure, 100%)	8 (11.1%)
Mixed (replacement, desmoplastic, or pushing)	25 (34.7%)
HGP1 (>50%) Predominant pattern	
Replacement (>50%)	54 (75%)
Desmoplastic (>50%)	18 (25%)
HGP2 (100%) Pure desmoplastic pattern	
Pure desmoplastic (100%)	8 (11.1%)
Any replacement (>5%)	64 (88.9%)
HGP3 (100%) Pure replacement	
Pure replacement (100%)	39 (54.2%)
Any desmoplastic (>5%)	33 (45.8%)

(16%) and 1 (2%) of the primary tumors, respectively. Genetic analysis revealed: D3/8 N: 3 patients (5%), M3/8 N: 5 (8%), D3/8 G: 18 (29%), M3/8 G: 36 (58%). A BAP1 mutation was present in 39 cases (69.6%).

Categorization of metastases by histopathological growth pattern (HGP)

Classification of the liver metastases by type and proportion of HGP is summarized in Table 2. Initial independent blinded review of the HGP in the 72 metastases by the two pathologists revealed good to excellent general agreement for 59 cases, whereas 13 cases (18% of the 72 cases) resulted in some discordance. The pathologists reached concordance by replacement of suboptimal glass slides or images and/or by webinar discussion and final consensus. The metastases were classified into four categories (Table 2). Pure vs Mixed: 39 metastases (54.2%) had a pure (100%) rHGP, 8 metastases (11.1%) a pure (100%) dHGP, and 25 (34.7%) a mixed pattern (admixture of replacement, desmoplastic, or pushing). For statistical analysis, the metastases were categorized as HGP1, HGP2, and HGP3: Predominant pattern (HGP1): 54 metastases (75%) were predominant (>50%) rHGP and 18 metastases (25%) predominant (>50%) dHGP. Pure (100%) dHGP (HGP2): 8 metastases (11.1%) pure (100%) dHGP, and 64 metastases (88.9%) any (>5%) rHGP. Pure (100%) rHGP (HGP3): 39 metastases (54.2%) pure (100%) rHGP and 33 (45.8%) any dHGP.

Whether predominant (>50% of the circumference of the metastasis) or pure, the rHGP was the most frequent pattern in this study. These metastases were characterized by nondestructive infiltration of the surrounding liver hepatic plates, progressive replacement of hepatocytes by melanoma cells (Fig. 1A) and preservation of the liver architecture (Fig. 1B). Individual and small aggregates of melanoma cells were aligned along the external (abluminal) surfaces of the sinusoidal vascular channels, corresponding to the Space of Disse (Fig. 1C, D).

A predominant or pure dHGP was recorded in 18 (25%) of cases and 8 (11.1%), respectively. These tumors were well-circumscribed with complete separation of the metastasis from the surrounding liver parenchyma by a dense band of desmoplastic collagen of variable width (Fig. 1E, F).

Mixed HGP metastases were seen in 25 (34.7%) cases and were classified as any rHGP (HGP2) or any dHGP (HGP3) (Table 2) [5]. The pushing HGP occurred in 10 cases and involved only a small fraction of the circumference of the metastasis: ranging from 5 to 25% with a prevailing dHGP or rHGP, or combination of the two.

L1CAM and laminin results and relationship to melanin index

Twenty-eight MUM were studied for L1CAM and laminin expression (Fig. 2). Twenty MUM had a pure (17) or predominate (3) rHGP, whereas, 8 cases exhibited a pure (2) or predominate (6) dHGP (Table 3). The melanin index was recorded in all 28 metastases.

L1CAM showed positive expression at the advancing front of 14/20 metastases with the replacement pattern ($p = 0.014$) (Fig. 2A, B) and was negative in the desmoplastic component and in the adjacent liver parenchyma of all 8 cases with a predominant or pure dHGP ($p = 0.014$) (Fig. 2C, D). In all rHGP metastases, L1CAM primarily labeled melanoma cells extending in a nondisruptive manner into the surrounding liver parenchyma as individual cells or small clusters of cells aligned along the surfaces of sinusoidal vascular channels. In some cases, as already mentioned, tumor cells extended up to 2 to 3 mm away from the metastasis proper. If L1CAM was noted within the metastasis, there was usually a gradient of diminution or loss of expression toward the center.

Another striking finding was the inverse relationship between L1CAM expression and the melanin index of each replacement pattern MUM ($p = 0.012$). L1CAM was either diminished or negative in 12 cases with a rHGP MUM and high melanin index (Fig. 2I). Among six cases with diminished scores of 2+ L1CAM, the melanin index was high, and among 6 cases negative for L1CAM, a maximum melanin index of 400 was registered in 4 of 6 cases. In some cases, melanin pigment was diminished or lost progressively from the center of the MUM to the advancing front and this was accompanied by an inversely progressive increase in L1CAM expression toward the periphery (Fig. 2J). A comparable inverse relationship of melan-A expression and melanin content was noted.

A "laminin vascular network" 4+ pattern was recorded in 16 of 20 MUMs with rHGP ($p = 0.000065$) (Fig. 2E, F); whereas, the dHGP component was negative for this finding in 8 of 8 MUMs ($p = 0.000063$) (Fig. 2G, H). The laminin vascular network was most conspicuous at the replacement advancing front and was in general lost or diminished toward the center of the MUMs. In addition, in five MUMs with predominate dHGP (65%, 85%, 90%, 95%, 95%), a laminin vascular network was localized to the smaller replacement component. However, L1CAM was negative in the latter desmoplastic components. Furthermore, this pattern of laminin immunostaining was preserved despite the high melanin index observed in the majority of the MUM with replacement pattern. It is of interest that method or degree of fixation appeared to influence significantly the expression of laminin. With a change in fixation from alcohol acetic acid formalin to formalin 4%, a loss of laminin network staining was observed in three replacement MUMs. A fourth case with loss of laminin staining appeared related to the age of the tissue block or other unexplained factors.

Approximately one-half of the 28 MUMs studied exhibited a melanin index of 200 or higher. As previously noted above, there appears to be a relationship between a low melanin index and the rHGP. Nonetheless, as just mentioned, high melanin index, i.e., ≥ 160 appears to correlate with diminished or absence of expression of L1CAM in the rHGP. There appeared to be no relationship between laminin and the melanin index ($p = 0.35$).

Although there appears to be a clear relationship between L1CAM and laminin vascular network in the rHGP, a Fisher's Exact test was not significant ($p = 0.102$).

Relationship between histopathological growth patterns and genetic and other prognostic factors (see Supplementary information)

Survival analysis results

Metastasis-free survival (MFS): The results of analysis of MFS are shown in Table 4. The mean and median MFS were 46 and

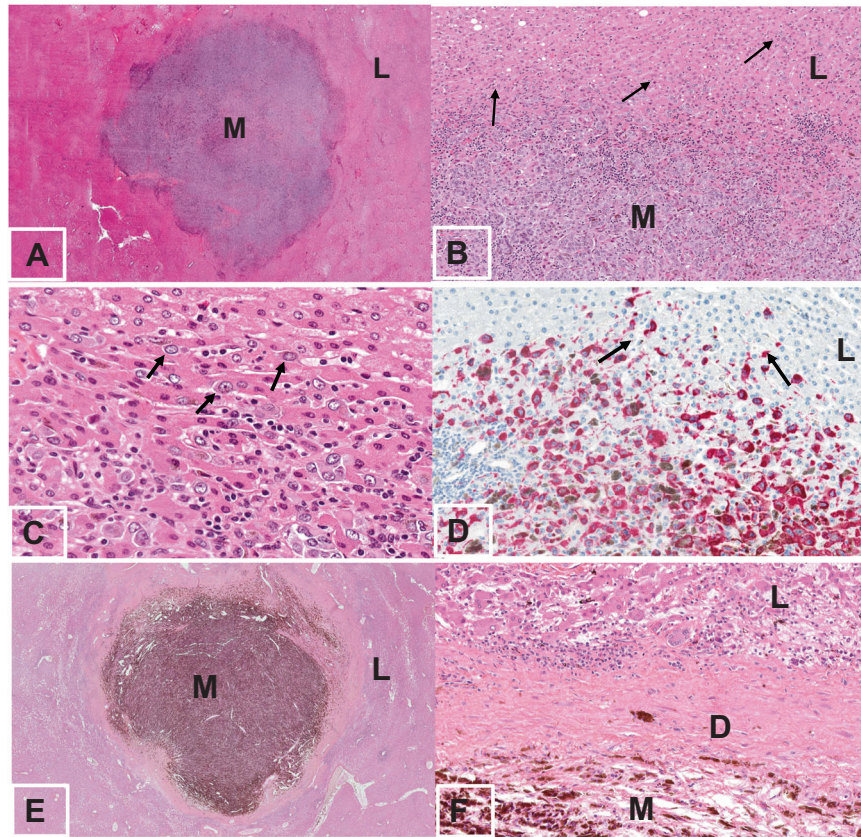


Fig. 1 Replacement and desmoplastic histopathological growth patterns in uveal melanoma liver metastases. Replacement histopathological growth pattern. A Scanning magnification shows a discrete metastasis (M) with surrounding uninvolved liver parenchyma (L). **B** The interface between the metastasis proper (M) and the overlying liver parenchyma (L) is a poorly-defined broad zone. Melanoma cells are dispersed throughout this interface as single cells (arrows) and in small clusters. These cells replace hepatocytes in the hepatic plates without altering their architecture. **C** Melanoma cells (arrows) extending into the surrounding hepatic plates some distance from the metastasis along the sinusoidal vessels. **D** HMB45 immunostain with red chromogen highlights melanoma cells extending into the surrounding liver parenchyma. **Desmoplastic histopathological growth pattern. E** Small round metastasis (M) with abrupt desmoplastic interface separates the tumor from the surrounding liver parenchyma. **F** An annulus of dense desmoplastic collagen constitutes this interface. Liver parenchyma (L) is observed in the upper half of this field and the metastasis (M) in the lowermost portion of the field. Note the rim of peritumoral lymphocytes, which are at the interface of the desmoplastic annulus (D) and the surrounding liver parenchyma.

31 months, respectively, with a range of 7–284 months. Based on binomial regression analysis, patients with monosomy 3 had significantly diminished mean and median intervals to the development of liver metastases versus those with disomy 3 ($p = 0.018$) (Fig. 3A). In contrast, BAP1 loss versus BAP1-wild type, as assessed by immunohistochemistry failed to demonstrate any reduction in MFS. The replacement HGP1, HGP2, and HGP3 showed a striking trend to diminished MFS compared to the desmoplastic pattern and which was significant for 100% replacement HGP3 (binomial regression: $p = 0.040$; Kaplan-Meier: $p = 0.05$). (Fig. 3B, C, D).

Metastasis-specific overall survival (MSOS) with reference to histopathological growth patterns and other variables: MSOS after the development of liver metastases averaged 30.8 months with a median of 23.4 months and range of 0 to 106 months. The effects HGP on MSOS were examined. The replacement pattern when analyzed as one of the three categorical variables: (1) HGP1: predominate rHGP (>50% rHGP), (2) HGP2: pure rHGP (100% rHGP), and (3) HGP3: any rHGP (>5% rHGP) had a clearly adverse effect on survival versus dHGP (Kaplan-Meier plots: $p = 0.0058$, $p = 0.038$, and $p = 0.0064$, respectively) (Fig. 4A, B, C). When analyzed as a continuous variable, rHGP remained significant ($p = 0.00$). Next, all clinical, genomic, and histopathologic prognostic variables were analyzed with the log-rank test (Supplementary

Table 4). The variables having significant predictive value for MSOS on univariate analysis were HGP1, HGP2, HGP3, and rHGP continuous (HR = 2.8, $p = 0.02$; HR = 3.4; $p = 0.091$; HR = 2.2, $p = 0.015$, HR = 1.0, $p = 0.005$, respectively); age ($p = 0.03$); primary tumor diameter (LTD) ($p = 0.04$); and R2 (versus R0 complete resection) status ($p = 0.000$); and best supportive care vs surgery alone ($p = 0.004$). No genetic variable including the genetic risk groups, monosomy 3, BAP1 mutation, or arrayCGH groups had any prognostic effect, nor did any of the other variables including gender, melanoma cell type, and melanin index (Supplementary Figs. 1, 2). Nonetheless, there was trend of aCGHr2 toward a prognostic effect ($p = 0.078$) (Supplementary Table 4).

On multivariate analysis with the log-rank test, HGP1, HGP2, and HGP3 continued to show significant Hazard Ratios (HR) of 5, 3.5, and 4.2 with $p = 0.02$, $p = 0.2$, $p = 0.04$, respectively (Supplementary Table 5). No other prognostic factors were significant.

Overall survival with reference to histopathologic growth patterns and other variables: (Supplementary information, Fig. 4D, E, F. Supplementary Tables 6 and 7).

DISCUSSION

We report for the first time that both L1CAM and laminin, defined as “laminin vascular network” are characteristically seen

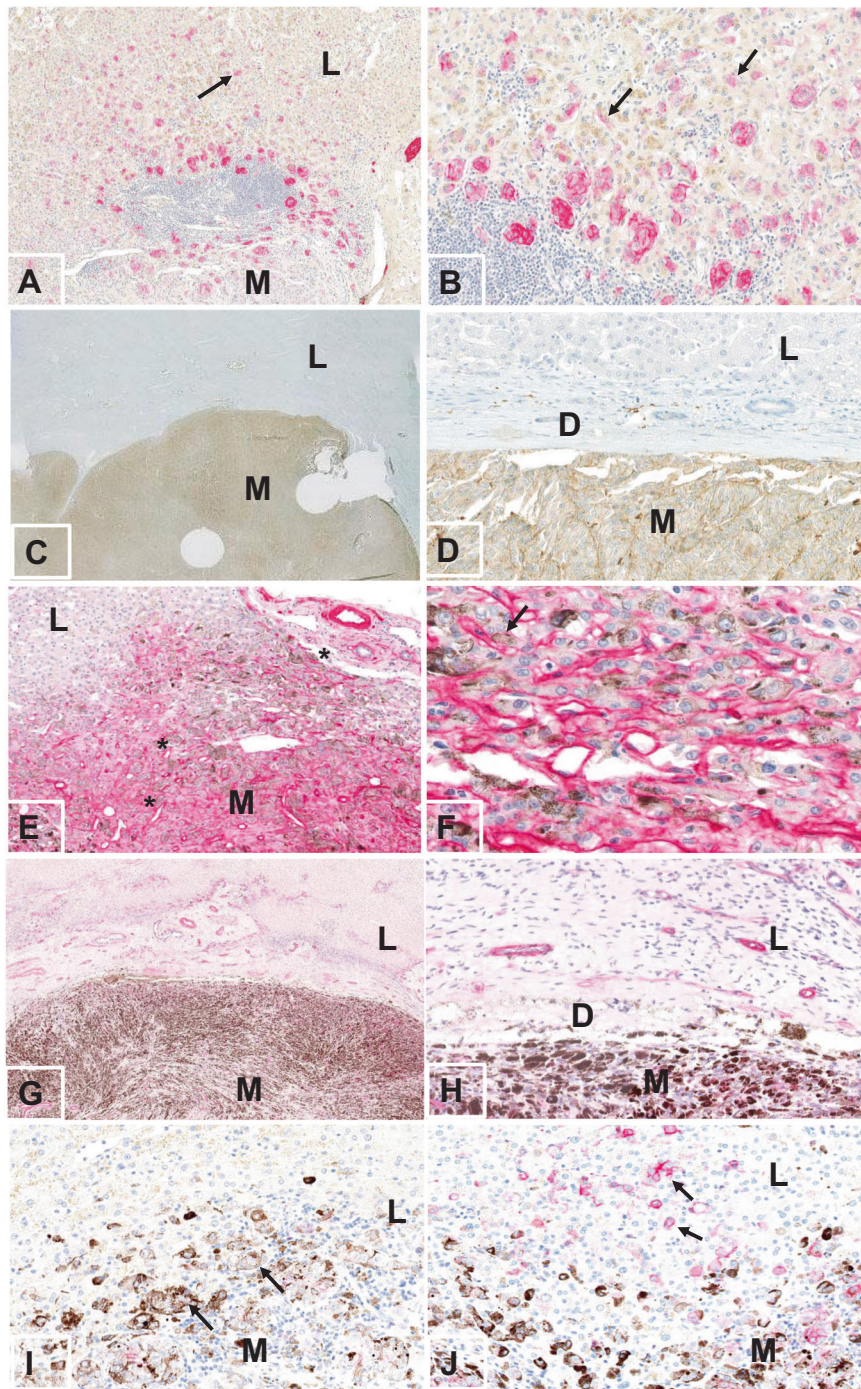


Fig. 2 L1CAM and laminin expression in uveal melanoma liver metastases. **L1CAM expression in HGPs.** **A** Replacement HGP. This field shows scattered nests of melanoma cells positive for L1CAM (red chromogen), seen predominately at the advancing front of the metastasis (M) with extension for some distance into the surrounding liver parenchyma (L). **B** The melanoma cells infiltrate among hepatocytes along the external surfaces of sinusoidal vascular channels in a non-infiltrative pattern. Note membranous expression of L1CAM. **C, D** Desmoplastic HGP. Absence of expression of L1CAM. **Laminin expression in HGPs.** **E** Replacement HGP. Laminin is strikingly positive in the infiltrative front and is characterized by a “vascular network pattern”, i.e., laminin marks (red chromogen) the basement membrane zone of anastomosing sinusoidal channels that interface with melanoma cells infiltrating the hepatic parenchyma. **F** This field shows scattered melanoma cells present along vascular channels positive for laminin (red chromogen) seen predominately at the advancing front of the metastasis. **G, H** Desmoplastic HGP. The prototypic laminin vascular network pattern is not seen. **I** Replacement HGP. High melanin index and general absence of L1CAM positivity in melanoma cells (arrows) at the advancing front. **J** Replacement HGP. Increasing L1CAM expression in melanoma cells (arrows) infiltrating the hepatic parenchyma (L) at the invasive front. These tumor cells exhibit diminished or absent melanin.

Table 3. L1CAM and laminin expression in replacement and desmoplastic growth patterns and influence of melanin index.

	HGP (%)			L1CAM	Laminin	Melanin index
	Replacement	Desmoplastic	Pushing			
1	100%			4+	4+	0
2	100			4+	Inadequate*	30
3	100			4+	Inadequate*	180
4	85	15		4+	Inadequate*	0
5	100			2+	4+	360
6	100			Negative	4+	400
7	90	10		Negative	4+	90
8	100			4+	4+	140
9	100			4+	4+	0
10	100			2+	4+	240
11	100			Negative	4+	400
12	100			Negative	4+	400
13	100			2+	4+	160
14	100			4+	4+	10
15	100			Negative	4+	400
16	100			2+	Inadequate*	360
17	100			2+	4+	400
18	100			4+	4+	15
19	60	40		2+	4+	400
20	100			Negative	4+	200
21	10	65	25	Negative	Negative**	280
22		100		Negative	Negative	400
23	15	80	5	Negative	Negative	0
24	5	95		Negative	Negative**	280
25	5	95		Negative	Negative**	0
26	10	90		Negative	Negative**	60
27		100		Negative	Negative	400
28	15	85		Negative	Negative**	0

*Inadequate preservation or change in fixative appears responsible for absence of laminin expressionNegative

**Absence of laminin vascular network pattern in desmoplastic component, laminin vascular network pattern may be seen in focal replacement component

Table 4. Metastasis-free survival (time to metastases, months) with reference to, chromosome 3 status, BAP1 mutation, and histopathologic growth patterns.

	Mean (sd)	Median (range)	p Value
All patients	46 (47.4)	31 (7–284)	NA
Monosomy 3	36.0 (30.5)	25 (7–125)	<i>p</i> = 0.018
Disomy 3	66.2 (67.8)	43 (8–284)	
BAP1 mutant	38.6 (31.5)	25 (7–125)	<i>p</i> = 0.509
BAP1 wild-type	45.9 (66.3)	20 (7–284)	
Histopathological growth pattern			
rHGP1	41.0 (38.7)	25 (7–143)	<i>p</i> = 0.379
dHGP1	58.2 (70.1)	42 (7–284)	
rHGP2	44.8 (49.2)	25 (7–284)	<i>p</i> = 0.461
dHGP2	53.2 (38.6)	54.5 (7–108)	
rHGP3	35.4 (35.5)	21 (7–141)	<i>p</i> = 0.040
dHGP3	56.6 (57.9)	42 (7–284)	
rHGP- Replacement HGP			
dHGP- Desmoplastic HGP			

at the advancing front of the rHGP of MUM. These observations provide new information about the biological basis of this phenomenon and serve as markers for the rHGP and angiotropic EVMM. Of particular note, L1CAM highlights angiotropism and the progressive extension of melanoma cells along the external surfaces of sinusoidal vessels in a pericytic

location, i.e., pericytic mimicry, some distance into the hepatic parenchyma, compared to its absence in the dHGP. On the other hand, laminin labels the basement membrane zone interposed between the abluminal surface of vascular channels and angiotropic melanoma cells at the advancing front of the tumor. We believe these observations are comparable with those in

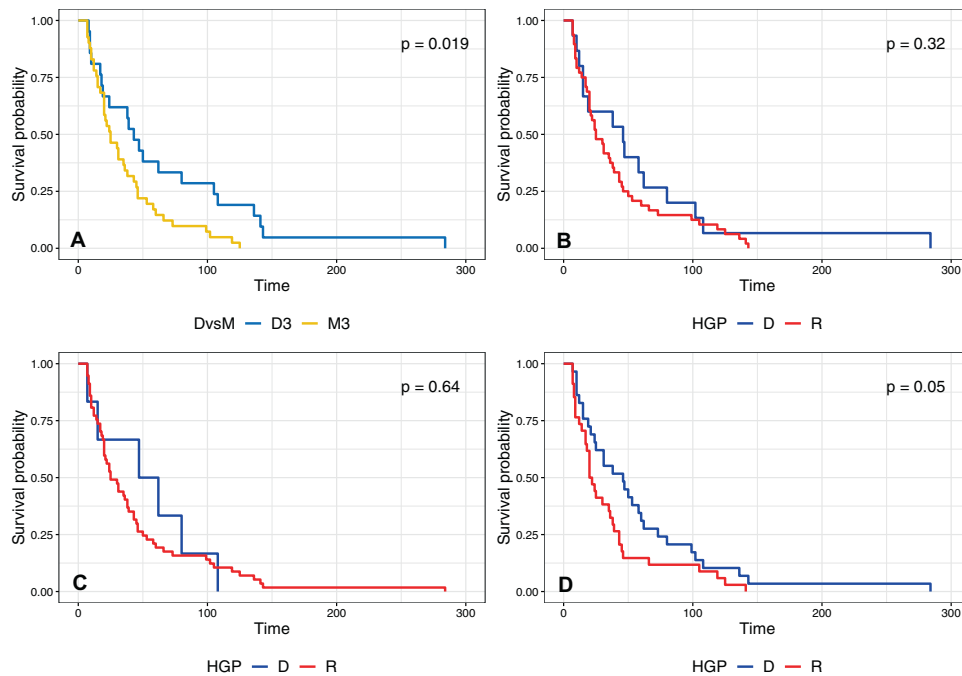


Fig. 3 Metastasis-free survival with reference to chromosome 3 status and histopathological growth patterns in uveal melanoma liver metastases. **A** Metastasis-free survival with reference to monosomy 3 and disomy 3 in 63 patients. **B** Metastasis-free survival and histopathological growth patterns in 63 patients: HGP1, predominate >50% rHGP vs >50% dHGP. **C** Metastasis-free survival and histopathological growth patterns in 63 patients: HGP2, any (>5 to 100%) rHGP vs 100% dHGP. **D** Metastasis-free survival and histopathological growth patterns in 63 patients: HGP3, 100% rHGP vs any (>5%) dHGP.

cutaneous melanoma, glioma, and other solid tumors (reviewed in 7) in identifying angiotropic extravascular tumor cell migration.

L1CAM, originally described as neuronal cell adhesion molecule, is now recognized as an important prognostic factor in many cancers¹¹. Of particular interest, it plays a crucial role in the spreading of tumor cells along vascular surfaces at the advancing front of metastases in experimental models of cancer metastasis. This phenomenon of tumor cell outgrowth corresponds to our earlier description of pericytic mimicry¹⁵. In addition, L1CAM has been detected in cancer cells that were near to vascular channels of a breast cancer dermal metastasis¹⁵. Recently, the same team has reported increased expression of L1CAM in colorectal cancer liver metastases as compared to matched primary tumors¹⁶. To our knowledge, our findings are the first to clearly demonstrate L1CAM expression by angiotropic melanoma cells aligned along the abluminal surfaces of vascular channels at the advancing front of human UM liver metastases with the rHGP.

Tumor cells implicated in angiotropic EVMM have been described as metastasis-initiating cells²⁸, and recent data have suggested that L1CAM enables the adhesion of these metastasis-initiating cells to laminin-rich basement membranes¹⁶. With particular reference to the current study, the characteristic “laminin vascular network” localized to the advancing front of the rHGP has previously been recognized in our studies (reviewed in ref. 7). As we have originally described by electron microscopy, the basement membrane interposed between metastatic melanoma cells and endothelial cells had a thickened amorphous nature rather than its typical organized trilaminar structure²⁹. We termed the latter ultrastructural finding “the angio-tumoral complex”. Furthermore, the latter amorphous basement membrane material showed intense immunostaining with laminin, which “formed a lattice surrounding the vessels with radial projections into the adjacent tumor mass”³⁰, and hence represented the original depiction of the “laminin vascular network”.

For many years, laminin has been recognized as playing a fundamental role in development and cancer biology. In particular, we have been interested in how changes in laminin structure and function modulate extravascular cancer cell migration. Various laminin isoforms have been implicated in migration and metastasis^{31–34} and expression has been detected in liver metastases from colorectal cancer³⁴.

The recent concept of a continuum between angiotropic EVMM and the replacement pattern via vessel co-option/pericytic mimicry³⁵ describes this mechanism of tumor migration as a reversion to an embryogenesis-derived program⁷. It should be recalled that the hypothesis that cancer represents a reversion to embryogenesis dates back to 1859^{36–38}. Notably, in development and cancer, tissue-specific interactions with distinct laminins are required for mesenchymal-to-epithelial transitions³⁹. In addition, L1CAM plays critical roles in neuronal migration, axon growth and guidance in the development of the nervous system^{14,40}. Our results suggest an intimate relationship between L1CAM and laminin in phenotypic switching and the putative embryonic migratory phenotype associated with the rHGP⁴¹. Concerning a switch of gene expression when tumor cells engage in angiotropism and pericytic mimicry (i.e., replacement), a previous experimental study had shown the new expression of genes including CCL2, ICAM1, IL6, SELE, TRAF1, SERPINB2, CXCL6, PDGFB, EVX1 and CFDP1⁷. We have also showed that environmental inflammatory signals can increase tumor cell plasticity and promote embryonic cell phenotypes^{7,42,43}. This study indicated also that neutrophilic inflammation in ulcerated melanomas shifts melanoma cells towards a migratory phenotype, activates endothelial cells and fosters reciprocal melanoma–endothelial interactions, which together promotes angiotropic invasion and metastasis.

An unusual finding was the apparent difference between L1CAM and laminin expression in the context of a high melanin index and the rHGP. With reference to the variation in L1CAM expression as a function of tumor cell melanin content, it is

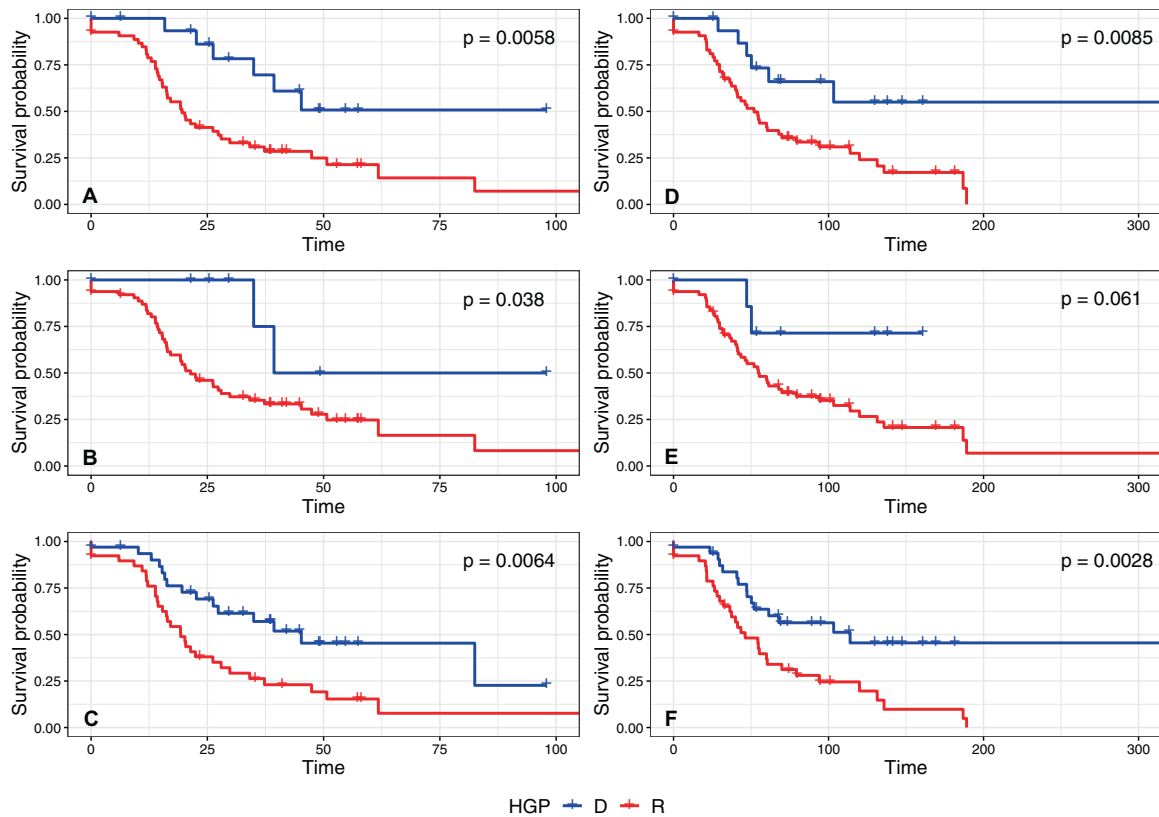


Fig. 4 Metastasis-specific survival and overall survival associated with histopathological growth patterns in uveal melanoma liver metastases. **A** Metastasis-specific overall survival associated with histopathological growth pattern groups in 72 patients with UM liver metastases. HGP1: predominate > 50% rHGP vs > 50% dHGP. **B** Metastasis-specific overall survival associated with histopathological growth pattern groups in 72 patients with UM liver metastases. HGP2: any (> 5 to 100%) rHGP vs 100% dHGP. **C** Metastasis-specific overall survival associated with histopathological growth pattern groups in 72 patients with UM liver metastases. HGP3: 100% rHGP vs any (> 5%) dHGP. **D** Overall survival associated with histopathological growth pattern groups in 72 patients with UM liver metastases. HGP1: predominate >50% rHGP vs >50% dHGP. **E** Overall survival associated with histopathological growth pattern groups in 72 patients with UM liver metastases. HGP2: any (>5 to 100%) rHGP vs 100% dHGP. **F** Overall survival associated with histopathological growth pattern groups in 72 patients with UM liver metastases. HGP3: 100% rHGP vs any (>5%) dHGP.

possible that cytoplasmic melanin simply blocks the membranous and cytoplasmic expression of L1CAM as with other membranous or cytoplasmic epitopes, e.g., melan-A⁴⁴. However, the latter results and the association between low melanin index and the 100% rHGP, mentioned above, provides additional evidence suggesting an amelanotic L1CAM-positive embryonic migratory phenotype, shared by the rHGP and angiotropic EVMM. Although our global analysis of melanin index as a prognostic factor in UM was not significant, melanin synthesis is, nevertheless, a marker of melanoma cell differentiation versus the absence of melanin and L1CAM expression being indicative of a less-differentiated or undifferentiated state⁷. Due to the plasticity of melanoma cells in phenotypic switching at the tumor microenvironmental level, gross analysis of the overall degrees of pigmentation of the entire tumor or metastasis appear inappropriate to capture such very localized biological processes and prognostic effects. This is borne out by the fact that the prognostic effect (and, a priori, the critical biological properties) of the rHGP culminate from the analysis of the advancing front of the metastasis. Targeted studies are currently underway to assess more precisely such localized biological events and their prognostic effects.

Finally, the striking differences between the rHGP and dHGP suggest that the mechanisms of tumor spread leading to these two HGPs also could be very different. Herein we have demonstrated for the first time that the rHGP is associated with notably diminished intervals to the development of metastases

(MFS) (especially for HGP3 (100% replacement) $p=0.040$) versus the desmoplastic pattern. This clearly requires further study for confirmation and potentially has important implications with respect to mechanisms of tumor cell spread and metastasis.

In the case of the rHGP, tumor cells may arrive from the primary tumor to the liver without intravasation via angiotropic EVMM, and are thus already potentially well adapted to perivascular microenvironments. The slow progression toward the liver via a step-by-step migration along vessels also would explain the clinical latency observed between the primary and secondary tumors, as well as, the continued progression along the liver vascular niches, known to be associated with a worse prognosis. On the other hand, tumor cells in the desmoplastic pattern may arrive via express intravascular dissemination, and therefore are less adapted to the microenvironment, leading to what is termed “dormancy” and finally longer latencies between the arrival in the liver and the progression to metastases. The overall survival from the diagnosis of the primary tumor may depend upon the velocity of tumor cells during EVMM, on the one hand, and the interval of dormancy and liver adaptation on the other. In addition, tumor cells involved in the dHGP could potentially switch to the rHGP by replacing pericytes of neovessels during inflammation/ angiogenic vascularization^{7,45}. The latter perspective also could explain the fact that genetic alterations (including monosomy 3 or BAP1 mutation) seem to play no role in influencing prognosis once liver

metastases are present (previous study⁴ and supplementary data). Therefore, it is an argument for epigenetic rather than genetic influences at this stage of the disease.

Potential limitations of our study are that UM is a rare cancer, and it is difficult to accumulate a large cohort of resected liver metastases, as in colorectal or breast carcinoma. However, MUM is an excellent model for studying metastasis in general since the mechanism of angiotropic extravascular migratory metastasis, vascular co-option, and histopathological growth patterns are relevant to all cancers.

Other new findings from our study have shown that any percentage of rHGP and pure rHGP have a significant adverse effect on MSOS ($p = 0.038$; $p = 0.0064$) in addition to predominant rHGP ($p = 0.0058$). Knowledge concerning the type of histopathological growth pattern is useful since it immediately signals an adverse prognosis for patients with the rHGP versus one more favorable for those with the dHGP. Type of HGP also conveys information about the potential resectability^{46,47} of metastases, as metastases of the dHGP type are often well defined and few in number⁵; whereas, metastases of the rHGP are poorly defined, often numerous, and sometimes of the diffuse "military" type, i.e., unresectable⁴⁶. Although not yet confirmed, the dHGP may correlate with PD-L1 expression and the likelihood of responding to immunotherapy⁴⁸. On the other hand, the rHGP appears to connote greater likelihood of poor response to therapy.

It would be of great utility to identify HGP by noninterventive radiological imaging for prognostic and surveillance purposes. In preliminary studies, there is increasing evidence that CT and MRI imaging can potentially detect HGPs and in particular, the well-defined desmoplastic rim in liver metastases from colorectal carcinoma and uveal melanoma, respectively, but further studies are needed^{49–52}. In preliminary study of UM, the correlation of MRIs images with dHGP was moderate to good ($\kappa = 0.52$) (Servois V., personal communication, 2022).

In conclusion, we report for the first time the identification of L1CAM and the laminin vascular network in the rHGP. Further studies are underway to precisely define how L1CAM and the laminin vascular network are involved in the molecular and epigenetic signaling of this aggressive pathway of tumor progression. Finally, in addition to signifying an adverse prognosis, we have shown that the rHGP also is associated with a diminished metastasis-free interval.

DATA AVAILABILITY

The datasets generated during and/or analysed during the current study are available from the corresponding author on reasonable request.

REFERENCES

- Aughton K, Kalirai H, Coupland SE. MicroRNAs and uveal melanoma: understanding the diverse role of these small molecular regulators. *Int J Mol Sci* 21:5648 (2020)
- Bustamante P, Piquet L, Landreville S, Burnier JV. Uveal melanoma pathobiology: Metastasis to the liver. *Semin Cancer Biol* 71:65–85 (2021)
- Rowcroft A, Loveday BPT, Thomson BNJ, Banting S, Knowles B. Systematic review of liver directed therapy for uveal melanoma hepatic metastases. *HPB (Oxford)* 22:497–505 (2020)
- Barnhill R, Vermeulen P, Daelemans S, van Dam PJ, Roman-Roman S, Servois et al. Replacement and desmoplastic histopathological growth patterns: A pilot study of prediction of outcome in patients with uveal melanoma liver metastases. *J Pathol Clin Res* 4:227–240 (2018)
- Latacz E, Höppener D, Bohlok A, Leduc S, Tabariès S, Fernandez Moro C, et al. Histopathological growth patterns of liver metastasis: updated consensus guidelines for pattern scoring, perspectives, and recent mechanistic insights. *Br J Cancer In Press*, (2022).
- Latacz E, Caspani E, Barnhill R, Lugassy C, Verhoef C, Grünhagen D et al. Pathological features of vessel co-option versus sprouting angiogenesis. *Angiogenesis* 23:43–54 (2020)

- Lugassy C, Kleinman HK, Vermeulen PB, Barnhill RL. Angiotropism, pericytic mimicry and extravascular migratory metastasis: an embryogenesis-derived program of tumor spread. *Angiogenesis* 23:27–41 (2020)
- Barnhill R, van Dam PJ, Vermeulen P, Champenois G, Nicolas A, Rawson RV et al. Replacement and desmoplastic histopathological growth patterns in cutaneous melanoma liver metastases: frequency, characteristics, and robust prognostic value. *J Pathol Clin Res* 6:195–206 (2020)
- Drew J, Machesky LM. The liver metastatic niche: modelling the extracellular matrix in metastasis. *Dis Model Mech* 14:dmm048801 (2021)
- Lugassy C, Scolyer R, Long G, Menzies A, Mischel P, Barnhill RL. PDGFBR expression in anti-BRAF resistant melanoma: are angiotropic melanoma cells a source of BRAF resistance and disease progression? *J Cutan Pathol* 41: 159–160 (2014)
- Maten MV, Reijnen C, Pijnenborg JMA, Zegers MM. L1 cell adhesion molecule in cancer, a systematic review on domain-specific functions. *Int J Mol Sci* 20:4180 (2019)
- Hall H, Carbonetto S, Schachner M. L1/HNK-1 carbohydrate- and beta 1 integrin-dependent neural cell adhesion to laminin-1. *J Neurochem* 68:544–553 (1997)
- SenGupta, S., Parent, C.A. & Bear, J.E. The principles of directed cell migration. *Nat Rev Mol Cell Biol* 22:529–547 (2021)
- Abe K, Katsuno H, Toriyama M, Baba K, Mori T, Hakoshima T, Kanemura Y, Watanabe R, Inagaki N. Grip and slip of L1-CAM on adhesive substrates direct growth cone haptotaxis. *Proc Natl Acad Sci USA* 115:2764–2769 (2018)
- Er EE, Valiente M, Ganesh K, Zou Y, Agrawal S, Hu J et al. Pericyte-like spreading by disseminated cancer cells activates YAP and MRTF for metastatic colonization. *Nat Cell Biol* 20:966–978 (2018)
- Ganesh K, Basnet H, Kaygusuz Y, Laughney AM, He L, Sharma R et al. L1CAM defines the regenerative origin of metastasis-initiating cells in colorectal cancer. *Nat Cancer* 1:28–45 (2020)
- Sekiguchi R, Yamada KM. Basement membranes in development and disease. *Curr Top Dev Biol* 130:143–191(2018)
- Giannelli G, Falk-Marzillier J, Schiraldi O, Stetler-Stevenson WG, Quaranta V. Induction of cell migration by matrix metalloproteinase-2 cleavage of laminin-5. *Science* 277:225–228 (1997)
- Qin Y, Rodin S, Simonson OE, Hollande F. Laminins and cancer stem cells: Partners in crime? *Semin Cancer Biol* 45:3–12 (2017)
- Bressan C, Saghatelian A. Intrinsic mechanisms regulating neuronal migration in the postnatal brain. *Front Cell Neurosci* 14:620379 (2021)
- Matarredona ER, Pastor AM. Neural stem cells of the subventricular zone as the origin of human glioblastoma stem cells. Therapeutic implications. *Front Oncol* 9:779 (2019)
- Sun T, Patil R, Galstyan A, Klymyshyn D, Ding H, Chesnokova A et al. Blockade of a laminin-411-notch axis with CRISPR/Cas9 or a nanobiocjugate inhibits glioblastoma growth through tumor-microenvironment cross-talk. *Cancer Res* 79:1239–1251 (2019).
- McLean IW, Burnier MN, Zimmerman LE et al. Atlas of tumor pathology. Tumors of the eye and ocular adnexa. America Registry of Pathology, Armed Forces Institute of Pathology, Washington, DC, 1994.
- Barnhill RL, Ye M, Batistella A, Stern MH, Roman-Roman S, Dendale R, Lantz O et al. The biological and prognostic significance of angiotropism in uveal melanoma. *Lab Invest*. 97:746–759 <https://doi.org/10.1038/labinvest.2017.16> (2017)
- Ramtohl T, Ait Rais K, Gardrat S, Barnhill R, Román-Román S, Cassoux N et al. Prognostic implications of MRI melanin quantification and cytogenetic abnormalities in liver metastases of uveal melanoma. *Cancers (Basel)* 13:2728 (2021)
- Viros A, Fridlyand J, Bauer J, Lasithiotakis K, Garbe C, Pinkel D et al. Improving melanoma classification by integrating genetic and morphologic features. *PLoS Med*. 5:e120 (2018)
- Cassoux N, Rodrigues MJ, Plancher C, Asselain B, Levy-Gabriel C, Lumbroso-Le Rouic L et al. Genome-wide profiling is a clinically relevant and affordable prognostic test in posterior uveal melanoma. *Br J Ophthalmol* 98:769–774 (2014)
- Massagué J, Ganesh K. Metastasis-initiating cells and ecosystems. *Cancer Discov* 11:971–994 (2021)
- Lugassy C, Eyden BP, Christensen L, Escande JP. Angio-tumoral complex in human malignant melanoma characterised by free laminin: ultrastructural and immunohistochemical observations. *J Submicrosc Cytol Pathol* 29:19–28 (1997)
- Lugassy C, Dickersin GR, Christensen L, Karaoli T, LeCharpentier M, Escande JP et al. Ultrastructural and immunohistochemical studies of the periendothelial matrix in human melanoma: evidence for an amorphous matrix containing laminin. *J Cutan Pathol* 26:78–83 (1999)
- Govaere O, Wouters J, Petz M, Vandewynckel YP, Van den Eynde K, Van den Broeck A et al. Laminin-332 sustains chemoresistance and quiescence as part of the human hepatic cancer stem cell niche. *J Hepatol* 64:60917 (2016)
- Govaere O, Petz M, Wouters J, Vandewynckel YP, Scott EJ, Topal B et al. The PDGFR α -laminin B1-keratin 19 cascade drives tumor progression at the invasive front of human hepatocellular carcinoma. *Oncogene* 36:6605–6616 (2017)

33. Rousselle P, Scoazec JY. Laminin 332 in cancer: When the extracellular matrix turns signals from cell anchorage to cell movement. *Semin Cancer Biol* 62:149–165 (2020)
34. Qin Y, Shembrey C, Smith J, Paquet-Fifield S, Behrenbruch C, Beyit LM et al. Laminin 521 enhances self-renewal via STAT3 activation and promotes tumor progression in colorectal cancer. *Cancer Lett* 476:161–169 (2020)
35. Lugassy C, Vermeulen PB, Ribatti D, Pezzella F, Barnhill RL. Vessel co-option and angiogenic extravascular migratory metastasis: a continuum of tumour growth and spread? *Br J Cancer*. 126:973–980 <https://doi.org/10.1038/s41416-021-01686-2> (2022)
36. Virchow R (1858) Cellular pathology, special ed., 204–207. London: John Churchill (1859)
37. Cofre J, Abdelhay E. Cancer is to embryology as mutation is to genetics: hypothesis of the cancer as embryological phenomenon. *ScientificWorldJournal* 2017:3578090 (2017)
38. Aiello NM, Stanger BZ. Echoes of the embryo: using the developmental biology toolkit to study cancer. *Dis Model Mech* 9:105–114 (2016)
39. Pitsidianaki I, Morgan J, Adams J, Campbell K. Mesenchymal-to-epithelial transitions require tissue-specific interactions with distinct laminins. *J Cell Biol* 220:e202010154 (2021)
40. Itoh K, Fushiki S. The role of L1cam in murine corticogenesis, and the pathogenesis of hydrocephalus. *Pathol Int* 65:58–66 (2015)
41. Rodrigues M, Mobuchon L, Houy A, Alsafadi S, Baulande S, Mariani O et al. Evolutionary routes in metastatic uveal melanomas depend on MBD4 alterations. *Clin Cancer Res*. 25:5513–5524 (2019)
42. Lugassy C, Péault B, Wadehra M, Kleinman HK, Barnhill RL. Could pericytic mimicry represent another type of melanoma cell plasticity with embryonic properties? *Pigment Cell Melanoma Res*. 26:746–754 (2013)
43. Bald T, Quast T, Landsberg J, Rogava M, Glodde N, Lopez-Ramos D, Kohlmeyer J, Riesenberger S, van den Boom-Konijnenberg D, Hömig-Hölzel C, Reuten R, Schadow B, Weighardt H, Wenzel D, Helfrich I, Schadendorf D, Bloch W, Bianchi ME, Lugassy C, Barnhill RL, Koch M, Fleischmann BK, Förster I, Kastenmüller W, Kolanus W, Hölzel M, Gaffal E, Tüting T. Ultraviolet-radiation-induced inflammation promotes angiogenesis and metastasis in melanoma. *Nature*. 507:109–113 (2014)
44. Orchard GE, Calonje E. The effect of melanin bleaching on immunohistochemical staining in heavily pigmented melanocytic neoplasms. *Am J Dermatopathol* 20:357–361 (1998)
45. Hoek KS, Eichhoff OM, Schlegel NC, Döbbling U, Kobert N, Schaerer L, Hemmi S, Dummer R. In vivo switching of human melanoma cells between proliferative and invasive states. *Cancer Res* 68:650–656 (2008)
46. Mariani P, Piperno-Neumann S, Servois V, Berry MG, Dorval T, Plancher C, Couturier J, Levy-Gabriel C, Lumbroso-Le Rouic L, Desjardins L, Salmon RJ. Surgical management of liver metastases from uveal melanoma: 16 years' experience at the Institut Curie. *Eur J Surg Oncol*. 2009 35:1192–1197 (2009)
47. Frenkel S, Nir I, Hendler K, Lotem M, Eid A, Jurim O, Pe'er J. Long-term survival of uveal melanoma patients after surgery for liver metastases. *Br J Ophthalmol*. 93:1042–1046. (2009)
48. Rodrigues M, Mobuchon L, Houy A, Fiévet A, Gardrat S, Barnhill RL, Popova T, Servois V, Rampanou A, Mouton A, Dayot S, Raynal V, Galut M, Putterman M, Tick S, Cassoux N, Roman-Roman S, Bidard FC, Lantz O, Mariani P, Piperno-Neumann S, Stern MH. Outlier response to anti-PD1 in uveal melanoma reveals germline MBD4 mutations in hypermutated tumors. *Nat Commun*. 9:1866 (2018)
49. Starmans MPA, Buisman FE, Renckens M, Willemsen FEJA, van der Voort SR, Groot Koerkamp B, Grünhagen DJ, Niessen WJ, Vermeulen PB, Verhoef C, Visser JJ, Klein S. Distinguishing pure histopathological growth patterns of colorectal liver metastases on CT using deep learning and radiomics: a pilot study. *Clin Exp Metastasis* 38:483–494 (2021)
50. Cheng J, Wei J, Tong T, Sheng W, Zhang Y, Han Y, Gu D, Hong N, Ye Y, Tian J, Wang Y. Prediction of histopathologic growth patterns of colorectal liver metastases with a noninvasive imaging method. *Ann Surg Oncol*. 26:4587–4598 (2019)
51. Han Y, Chai F, Wei J, Yue Y, Cheng J, Gu D, Zhang Y, Tong T, Sheng W, Hong N, Ye Y, Wang Y, Tian J. Identification of predominant histopathological growth patterns of colorectal liver metastasis by multi-habitat and multi-sequence based radiomics analysis. *Front Oncol*. 10:1363 (2020)
52. Wei S, Han Y, Zeng H, Ye S, Cheng J, Chai F, Wei J, Zhang J, Hong N, Bao Y, Zhou J, Ye Y, Meng X, Zhou Y, Deng Y, Qiu M, Tian J, Wang Y. Radiomics diagnosed histopathological growth pattern in prediction of response and 1-year progression free survival for colorectal liver metastases patients treated with bevacizumab containing chemotherapy. *Eur J Radiol*. 142:109863 (2021)

AUTHOR CONTRIBUTIONS

RB and CL wrote the manuscript, RB, CL, PV developed the methodology, RB, CL, PV collected and analyzed data. SVL performed statistical analyses and analyzed data. GC and AN performed immunohistochemistry, scanned glass slides, and managed glass microslides. PM and SPN collected data. All the authors reviewed and approved the manuscript.

FUNDING

This work was supported by Uveal Melanoma (UM) Cure 2020 project under the European Union's Horizon 2020 research and innovation program (grant agreement No 667787)". Period 2015–2021. RAS is supported by an Australian National Health and Medical Research Council Practitioner Fellowship (APP1141295). Support from Deborah McMurtrie and John McMurtrie AM and The Cameron Family is gratefully acknowledged. The authors also acknowledge support from colleagues at their respective institutions.

COMPETING INTERESTS

The authors declare no competing interests.

ETHICS APPROVAL AND CONSENT TO PARTICIPATE

This study was approved by the institutional ethics committees of Curie Institute in Paris France; the Melanoma Institute of Australia; and The University of Texas MD Anderson Cancer Center. Written informed consent for the use of tissue specimens and data for research was signed by each patient.

ADDITIONAL INFORMATION

Supplementary information The online version contains supplementary material available at <https://doi.org/10.1038/s41374-022-00803-w>.

Correspondence and requests for materials should be addressed to Raymond Barnhill.

Reprints and permission information is available at <http://www.nature.com/reprints>

Publisher's note Springer Nature remains neutral with regard to jurisdictional claims in published maps and institutional affiliations.